Title

Uncovering the Role of Hole Traps in Promoting Hole Transfer from Multiexcitonic Quantum Dots to Molecular Acceptors

Journal

ACS Nano, 15(2)

ISSN

1936-0851

Authors

Yan, Chang
Weinberg, Daniel
Jasrasaria, Dipti
et al.

Publication Date

2021-02-23

DOI

10.1021/acsnano.0c08158

Peer reviewed

Uncovering the Role of Hole Traps in Promoting Hole Transfer from Multi-Excitonic Quantum Dots to Molecular Acceptors

Chang Yan[1,2], Daniel Weinberg[1,2], Dipti Jasrasaria[1], Matthew A. Kolaczkowski[1,3], Zi-jie Liu[1], John P. Philbin[1], Arunima D. Balan[1], Yi Liu[3], Adam M. Schwartzberg[3], Eran Rabani[1,2,6]*, and A. Paul Alivisatos[1,2,4,5]*

1. Department of Chemistry, University of California, Berkeley, California 94720, United States

2. Materials Sciences Division, Lawrence Berkeley National Laboratory, Berkeley, California 94720, United States

3. Molecular Foundry, Lawrence Berkeley National Laboratory, Berkeley, California 94720, United States

4. Department of Materials Science and Engineering, University of California, Berkeley, California 94720, United States

5. Kavli Energy NanoScience Institute, Berkeley, California 94720, United States

6. The Sackler Center for Computational Molecular and Materials Science, Tel Aviv University, Tel Aviv, Israel 69978

* Corresponding authors: paul.alivisatos@berkeley.edu; eran.rabani@berkeley.edu

Abstract

Understanding electronic dynamics in multi-excitonic quantum dots (QDs) is important for designing efficient systems useful in high power scenarios, such as solar concentrators and multi-electron charge transfer. The multiple charge carriers within a QD can undergo undesired Auger recombination events, which rapidly annihilate carriers on picosecond timescales and generate heat from absorbed photons instead of useful work. Compared to the transfer of multiple electrons, the transfer of multiple holes has proven to be more difficult due to slower hole transfer rates. To probe the competition between Auger recombination and hole transfer in CdSe, CdS, and CdSe/CdS QDs of varying sizes, we synthesized a phenothiazine derivative, with optimized functionalities for binding to QDs as a hole accepting ligand and for spectroscopic observation of hole transfer. Transient absorption spectroscopy was used to monitor the photo-induced absorption features from both trapped holes and oxidized ligands under excitation fluences where the averaged initial number of excitons in a QD ranged from ~1 to 19. We observed fluence-dependent hole transfer kinetics that last around 100 ps longer than the predicted Auger recombination lifetimes, and the transfer of up to 3 holes per QD. Theoretical modeling of the kinetics suggests that binding of hole acceptors introduces trapping states significantly different from those in native QDs passivated with oleate ligands. Holes in these modified trap states have prolonged lifetimes, which promotes the hole transfer efficiency. These results highlight the beneficial role of hole trapping states in devising hole transfer pathways in QD-based systems under multi-excitonic conditions.

Keywords: quantum dots, hole transfer, multi-excitonic states, Auger recombination, charge trapping, surface ligands.

Introduction

Due to their size-dependent electronic structure, tunable composition, high absorptivity, and remarkable photostability, colloidal quantum dots (QDs) have found diverse applications in light-emitting devices,[1,2] biological imaging,[3,4] solar harvesting technologies,[5,6] and photocatalysis.[7,8] QDs as light absorbers in colloidal solutions have been studied extensively to drive photochemical reactions by transferring excited state energy or photo-generated charges to neighboring acceptors.[9] In recent works, the scope of QD photochemistry has been expanded rapidly beyond the efficient H_2 evolution from aqueous solutions,[7,10,11] including examples such as CO_2 reduction,[12,13] 2+2 cycloaddition,[14] carbon-carbon bond formation,[15] and radical polymerization.[16]

One of the unique features of QDs, as compared to molecular light absorbers, is their capacity to concentrate many excited charge carriers within a small volume following multiple photon absorption or charge multiplication processes, due to their large absorptivity and high density of available electronic states.[17,18] The multi-excitonic state of a QD can enable photophysical processes that are inaccessible by single-excitonic states, such as the transfer of multiple charges on ultrafast timescales[19,20] and the tunneling transport of electrons across high energy barriers.[21] The efficient extraction of charge carriers from multi-excitonic QDs would also be particularly useful for reactions related to photocatalytic solar fuel generation, as these chemical transformations universally involve multi-electron catalysis.

As depicted in Figure 1A, the multi-excitonic state of a QD can undergo multi-excitonic dissociation (MED) to transfer charges to acceptors, thereby creating a charge-separated state, which generally has a long lifetime. However, as the excitons are confined in the small volume of a nanocrystal, the Coulomb interaction between multiple excitons unavoidably leads to Auger

recombination (AR), which non-radiatively annihilates an exciton and creates a hot electron-hole pair. The AR rate increases nonlinearly with the number of excitons in a QD.[18] On fast timescales from several to hundreds of picoseconds (ps, 10^{-12} second), AR can swiftly annihilate charge carriers until the QD is brought to the single-excitonic state.[18] Hole transfer rates are typically much slower, and yet ideally QDs could be designed such that, when multiply excited, hole transfer could still compete efficiently against AR.

Ultrafast multiple electron transfer occurring within a few picoseconds has been observed to compete effectively against AR events in a number of systems, including CdS QDs,[22] CdSe QDs,[23,24] CdSe/CdS core/shell QDs,[19] and PbS QDs.[25] In contrast, the transfer of multiple holes from a QD to acceptors is typically much more challenging and had not been observed until a recently reported case, where up to 5.6 holes were extracted from a $CsPbCl_xBr_{3-x}$ QD to tetracene acceptors.[26] As the inefficient part of the redox cycle, hole transfer processes often form the bottleneck for improving the overall performance of photocatalysts and photovoltaic devices.[27] Furthermore, the accumulation of holes on the widely studied metal chalcogenide QDs leads to their eventual photo-degradation.[28] Therefore, it is very desirable to provide mechanistic insights for devising pathways that could efficiently extract multiple holes from a QD.

For metal chalcogenide QDs, hole trap states are prevalent on the surface due to under-passivated chalcogenide atoms.[29,30] The multitude of these relatively localized hole traps play an important role in mediating hole transfer from delocalized valence band (VB) states to surface bound acceptors.[31–33] Hole trapping states also affect the AR lifetimes by altering the electron-hole interactions and, therefore, significantly impacting the kinetic competition between hole transfer and AR dynamics.[34–36] Ultrafast transient absorption (TA) spectroscopy provides the time resolution required to directly track the population of holes in different states as they

migrate from QDs to acceptors. Previous work with TA methods by Lian *et al.* and Weiss *et al.* have established that phenothiazine derivatives can serve as a class of hole acceptors for CdS QDs or nanorods with both the high driving force and the necessary optical signature in TA to track hole transfer.[31,37,38] In these model systems, ultrafast hole trapping was observed within ~1 ps following photo-excitation, and trap-mediated hole transfer dynamics were investigated under single-excitonic or bi-excitonic conditions.

Herein, we utilized TA spectroscopy to investigate the hole transfer dynamics from three different cadmium chalcogenide QDs to a synthesized phenothiazine derivative, which binds to the QD surface via a carboxylate group (Figure 1B). The QDs were excited by a pump pulse of 415 nm wavelength and the average initial number of excitons per QD, $\langle N_0 \rangle$, was experimentally calibrated to range from ~1 to 19. The hole acceptor, 4-(3-bromo-7-(dihexylamino)-10H-phenothiazin-10-yl)-benzoic acid (NPTZ), is designed to carry functional groups on the phenothiazine ring to shift the photo-induced absorption (PA) signal of its oxidized form to the longer wavelength region > 600 nm. The shifted PA feature enables us to track the hole transfer in CdSe and CdSe/CdS QDs by avoiding interference with exciton bleaching (XB) signal.

In the QD-NPTZ systems, the time-dependent populations of the trapped holes and the oxidized ligands were separately tracked and analyzed so that we could systematically investigate the interplay between charge trapping, hole transfer, and Auger recombination dynamics. To describe the observed kinetics, we test two types of kinetic models where the hole trapping states are kinetically coupled to or de-coupled from the VB populations. For QDs passivated with oleate ligands (referred to as native QDs), our results indicate that the hole trapping states exist in a fast trapping/de-trapping equilibrium with the VB, and the trapped holes can be rapidly consumed by AR events. In contrast, the hole trapping states in QDs capped with

NPTZ ligands are kinetically de-coupled from VB states and have prolonged lifetimes. Fluence dependent hole transfer kinetics were observed at intermediate times of 10s to 100s of ps, after AR would be expected to relax the QDs to single-excitonic states. These de-coupled trapping states resemble the long-lived charge-separated states proposed to account for the 'dark states' in QD single particle blinking experiments.[39,40] The long-lived, trapped holes can serve as a reservoir to temporarily store charges, and then slowly transfer to NPTZ over the course of 10s to 100s of ps. In the most efficient system, up to 3 holes were transferred to NPTZ per CdS QD.

Figure 1. A) The Jablonski diagram of the QD-NPTZ system used to study multi-excitonic hole transfer

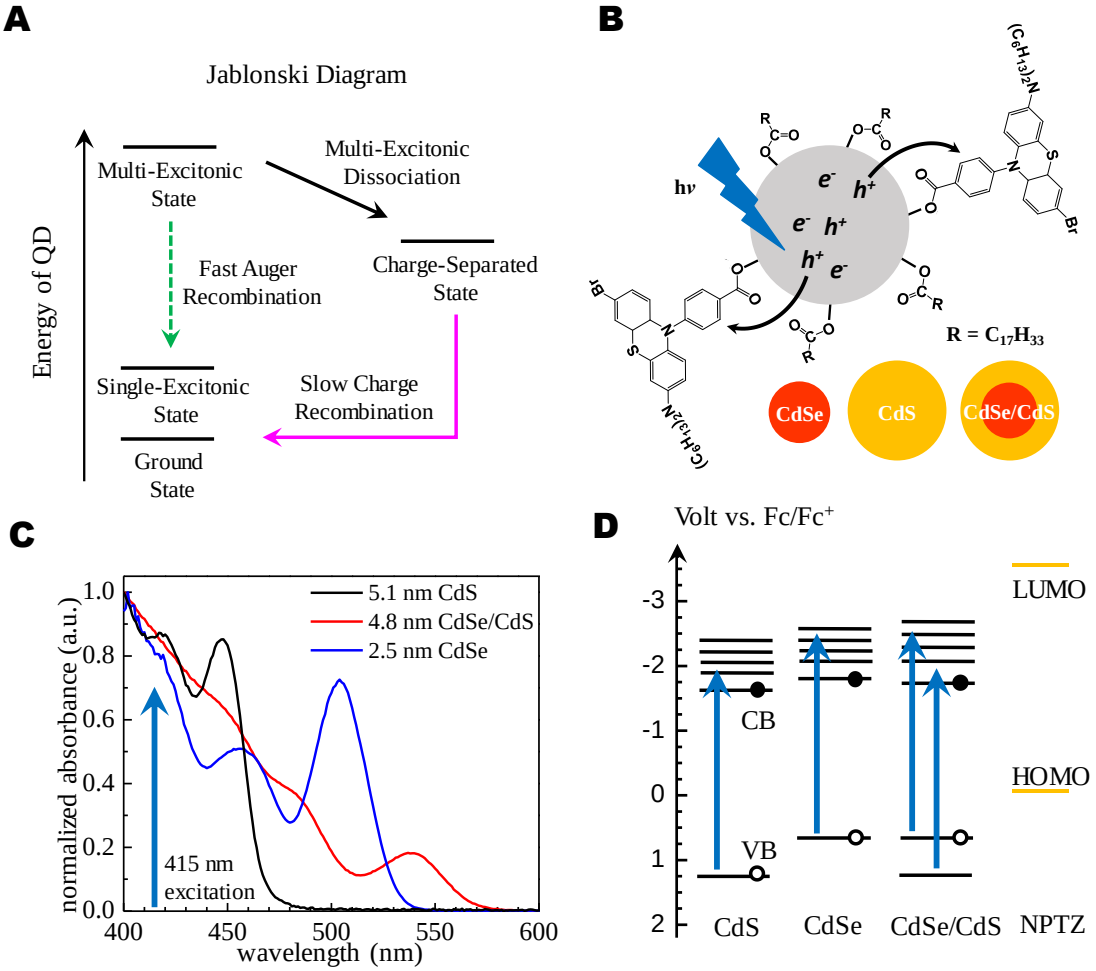

dynamics. The fast Auger recombination dynamics (green dashed arrow) competes with multi-excitonic dissociation dynamics (black arrow). **B)** Schematic illustration of multi-excitonic hole transfer from QDs to NPTZ ligands. **C)** Normalized absorption spectra of the investigated QDs dissolved in toluene. The excitation wavelength used in TA experiments was 415 nm (~3.0 eV). **D)** The diagram shows the energy levels of QDs and NPTZ ligand relative to the ferrocene/ferrocenium redox couple in acetonitrile.

Trapping states are omitted from the display. The scaled length of the blue arrows is 3.0 eV. For the core/shell system, both CdSe core and CdS shell contribute to photo-absorption.

Results/Discussions

Design of the TA Measurements and Major TA Spectral Features

To investigate the competition between hole transfer and AR kinetics, we examined a series of QDs of different sizes and compositions. As the AR lifetime of a QD generally increases with the volume of a QD,[18,41] we present the results obtained from the following systems: a small CdSe QD (d = 2.5 nm); a large CdS QD (d = 5.1 nm); and a core/shell CdSe/CdS QD (d_{total} = 4.8 nm, d_{core} = 2.3 nm) with a quasi-type II band structure. By exciting the QDs at the absorption band edge, the bi-excitonic AR rates were determined to be $(3.0\ ps)^{-1}$, $(22\ ps)^{-1}$, and $(35\ ps)^{-1}$ for the CdSe, CdSe/CdS, and CdS QDs studied here, respectively (Table S6).

To promote the transfer of multiple holes, the QDs were functionalized with the highest possible surface coverage of the NPTZ ligands. The NPTZ ligands replace the native oleate ligands in a 1-to-1 stoichiometry and bind to cadmium ions on the QD surface via their carboxylate group. The 1-to-1 stoichiometry and surface coverage of the NPTZ ligand can be determined by the ^{1}H nuclear magnetic resonance technique (Table S1). Because the NPTZ ligands are significantly larger molecules than the oleate ligands, the surface coverages of NPTZ ligands saturates at around 20% for all the QDs. For the 2.5 nm CdSe, we calculated that there are ~25 NPTZ ligands bound per QD. For the 5.1 nm CdS and 4.8 nm core/shell QD, there are ~75 NPTZ ligands bound per QD.

The UV-visible absorption spectra of the three types of QDs are shown in Figure 1C. In the TA experiments, the pump wavelength was set above the band edge energy of the QDs at 415 nm (~3 eV) to access levels deep in the energy bands and create a large number of excitons. The energy diagrams of the QDs and NPTZ are shown in Figure 1D. The absorption feature of the

phenothiazine ring located in the UV region (>3 eV) will not be excited (Figure S5).[31,38] The driving force of hole transfer from all three types of QDs to the NPTZ molecule is sufficiently high,[27] as the highest occupied molecular orbital (HOMO) of NPTZ is located 0.7 eV and 1.2 eV above the VB band edges of CdSe and CdS, respectively.[27] Photo-induced charge transfer from the QDs to NPTZ is energetically prohibited. The blue arrows in Figure 1D point to the highest possible conduction band (CB) levels to which the electrons can be promoted by the 415 nm excitation. These levels are significantly lower than the lowest unoccupied molecular orbital (LUMO) of NPTZ. The HOMO and LUMO positions of NPTZ were determined from cyclic voltammetry and UV-visible absorption spectroscopy (Figure S4).

Photoexcited hot electrons and holes rapidly cool on a sub-picosecond timescale to energy levels near the band edges, as shown by the solid and empty circles, respectively, in Figure 1D. The strongly quantum confined 2.5 nm CdSe QD and the weakly quantum confined 5.1 nm CdS QD differ significantly in the VB edge energies but have similar CB edge energies. For the 4.8 nm CdSe/CdS QD containing a 2.3 nm CdSe core, the 415 nm pump pulse excites both the CdSe core and the CdS shell. Due to the small size of the core, the energy levels of CdSe and CdS form a quasi-type II alignment causing the electron wave function to distribute throughout both the core and the shell while the hole wave function localizes mostly to the core after cooling.[19,42,43] In the core/shell system, the driving force for hole transfer is determined by the CdSe core, and the transfer to surface ligands needs to overcome the energy barrier of the CdS shell.[27,32]

We measured the TA spectra for a series of excitation fluences for both the native QDs capped with oleate ligands and the QDs with surface bound NPTZ ligands. For each TA measurement, the initial average number of excitons per QD, $\langle N_0 \rangle$, was experimentally determined from the calibrated energy per pump pulse, the effective absorbance at 415 nm for each pump pulse energy, the excited sample volume, and the concentration of QD in solution (Tables S2-S4). To reduce the spread of $\langle N_0 \rangle$ caused by the attenuation of the pump pulse through the sample while maintaining a reasonable signal level for TA experiments, the optical densities at 415 nm for all the samples were kept around 0.2. The relative standard deviation of the calculated $\langle N_0 \rangle$ is ~15% for all the samples.

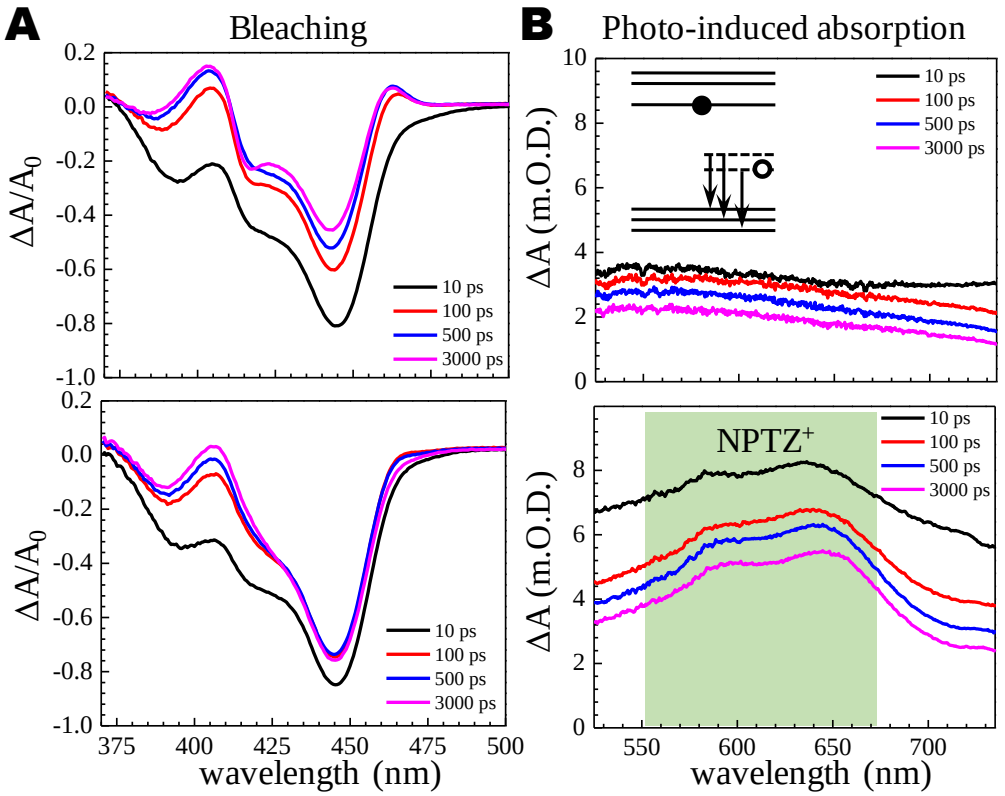

Figure 2. Examples of TA spectra at various delay times showing the exciton bleaching **(A)** and photo-induced absorption **(B)** features of CdS QDs without NPTZ (top panels) and with NPTZ (bottom panels) added. The excitation power is 1.25 μJ per pulse and $\langle N_0 \rangle \approx 19$. The inset in the upper panel of **(B)** indicates that the broad offset-like PA feature originates from the absorptions promoting the trapped holes into densely spaced levels deep in the VB. The green shaded area in the bottom panel of **(B)** highlights the PA peaks of $NPTZ^{+\bullet}$ radical on top of the PA feature of trapped holes.

In Figure 2, the TA spectra of CdS QDs with native oleate ligands and NPTZ ligands are displayed as examples to illustrate the major TA features used for kinetic analysis. The major negative XB feature around 450 nm shown in Figure 2A is associated with the bleaching of the first excitonic transition from $1S_h$ to $1S_e$ of the QD. The change of absorbance induced by the pump pulse, ΔA, was divided by the steady-state linear absorbance at the peak of the first excitonic absorption peak, A_0. The lowest CB level ($1S_e$ state) can accommodate at most two electrons, and therefore the XB signal at the band edge will be close to the saturation level of $\Delta A/A_0 \sim 1$ when the CB is populated by two or more electrons.[19,37] At the early time t = 10 ps, both the QDs with and without NPTZ ligands showed nearly full saturation of the band edge XB signal as seen by the black lines in Figure 2A. For QDs without NPTZ added (top panel), the XB signal decayed to $\Delta A/A_0 \sim 0.5$ at longer delay times t > 100 ps, indicating that fast AR processes have brought the system from a multi-excitonic state to a single-excitonic state. For CdS QDs bound with NPTZ ligands (bottom panel), the full saturation level lasts for several nanoseconds (ns), indicating that >2 electrons remain on the CB. For systems where less than 2 holes were transferred, we did not observe the lasting saturation of the band edge XB signals on ns timescales (Figures S14-S15). This XB signal cannot, however, be used to determine the dynamic behavior of the holes associated with these electrons. Tracking the hole population requires detailed analysis of other spectroscopic data discussed below.

In Figure 2B, the positive PA features of CdS are shown in the range of 535-735 nm. Based on theoretical[44] and experimental evidence,[19,45] this broad but weak PA signal is assigned to the transitions promoting trapped holes into deeper levels of the VB (inset in the upper panel of Figure 2B). The high density of states in the VB causes the broad feature of the PA signal. The hole trapping states in native QDs dispersed in colloidal solutions are typically attributed to

under-passivated surface chalcogenide atoms. The PA signal of trapped holes shares the same broad, offset-like feature for all the three types of QDs measured here. The transient kinetics of the trapped hole population are largely independent of the wavelength chosen for analyzing the PA signal (Figures S18-S19). To avoid overlapping with the PA signal of oxidized NPTZ ligands, we chose to use 710 nm as the wavelength for tracking the population of trapped holes because the signal amplitude at 710 nm was unaffected by the deconvolution of the contribution from the molecular acceptors. Hole transfer and AR of multi-excitonic states can be inferred from the decay kinetics of the broad PA feature. As discussed later, the decay kinetics of the population of trapped holes represented at 710 nm were qualitatively different for QDs with or without NPTZ ligands due to the altered nature of hole trapping states.

For NPTZ-capped QDs, the oxidation of NPTZ ligands by hole transfer gives rise to the absorption band in the region from 550-670 nm (green shaded area in Figure 2B). This PA band is assigned to the transiently generated $NPTZ^{+\bullet}$ radical, and the extinction coefficient of the PA peak at 650 nm was estimated from steady-state oxidation titrations (Figure S5). Compared to the phenothiazine molecule, the amine group and the bromine atom on the aromatic ring of NPTZ shifted the radical absorption peak from ~520 nm to 650 nm. For the CdSe and the core/shell QDs studied here, the shifted peak allows the radical PA signal to be resolved from the tails of the XB signal, which is larger in amplitude by orders of magnitude. For CdSe QDs larger than d = 3.5 nm or CdSe/CdS QDs larger than the one studied here, the XB signal would redshift enough to severely interfere with the $NPTZ^{+\bullet}$ radical signal.

The signal of the $NPTZ^{+\bullet}$ radical and the broad signal of trapped holes can be de-convoluted from each other by a fitting protocol (Figure S21).[31,38] The de-convoluted PA amplitude of $NPTZ^{+\bullet}$ at 650 nm directly tracks the average number of holes transferred per QD,

$\langle N_{HT} \rangle$, which was calculated by the ratio of the concentration of the $NPTZ^{+\bullet}$ radical to the concentration of QDs (Table S5).

To deepen our mechanistic understanding of the hole transfer process, we developed a kinetic model of the dynamics of the hole populations on both the native QDs and QDs with NPTZ hole acceptors. As discussed below for Figure 4, the kinetic model incorporates three hole populations: valence band holes, trapped holes, and holes transferred to NPTZ ligands. The population of trapped holes can be tracked with the broad PA signal at 710 nm, and the population of holes transferred to NPTZ ligands can be monitored by the 650 nm $NPTZ^{+\bullet}$ absorption band. While the population of valence band holes cannot be measured directly in the optical range of our experiments, it can be inferred from the initial excitation conditions. The processes of trapping, de-trapping, AR, and hole transfer connect these hole states and give rise to the complex dynamic behaviors we observe and simulate within our kinetic model.

Hole Transfer Kinetics and Quantum Yields Measured from PA Signals of $NPTZ^{+\bullet}$

In Figure 3A-3C, the de-convoluted kinetics of $NPTZ^{+\bullet}$ at 650 nm are shown in the time range from 5 ps to 7 ns for the three QD systems studied here. For conditions with large $\langle N_0 \rangle$, the broad PA signal background from QDs measured prior to t = 5 ps has time-dependent slopes, which are difficult to analyze, so that data are not shown here. The pump pulse energies applied for each type of QD are in the interval between 0.07 μJ and 1.27 μJ per pulse. For CdS QDs and CdSe/CdS core/shell QDs, the excitation energies produce an $\langle N_0 \rangle$ ranging from ~2 to 19. Due to their smaller molar extinction coefficient at 415 nm, the $\langle N_0 \rangle$ for the CdSe QDs ranges from 0.5 to 4.4.

The kinetic plots in Figure 3A-3C show that the photo-excited dynamics of a QD with NPTZ under multi-excitonic conditions take place on multiple timescales. In the first ~10 ps, the CdS QDs (Figure 3A) display a very rapid initial increase in the $NPTZ^{+\bullet}$ signal, whereas the hole transfer signal of the other two QDs is insignificant in this time period. After ~10 ps, all the QD systems exhibit an exponential increase in the $NPTZ^{+\bullet}$ signal over the next ~100 ps. In the period from 1-7 ns, the hole transfer rate approaches zero for all QD systems. The population of transferred holes is generally stable with long charge-separation lifetimes. For the systems where multiple holes are transferred at high excitation fluences, the $NPTZ^{+\bullet}$ signals decay due to charge recombination between the radical and QDs on this long timescale, e.g., the pink trace of CdS in Figure 3A. For the CdS QDs, the transfer of multiple holes with $\langle N_{HT} \rangle$ >2 was observed at the conditions of high $\langle N_0 \rangle$. For the CdSe and CdSe/CdS QDs, more holes were transferred as the excitation fluence was increased, but overall fewer than two holes were transferred from a QD to NPTZ molecules. The solid lines are modeling results, which will be discussed in the next section.

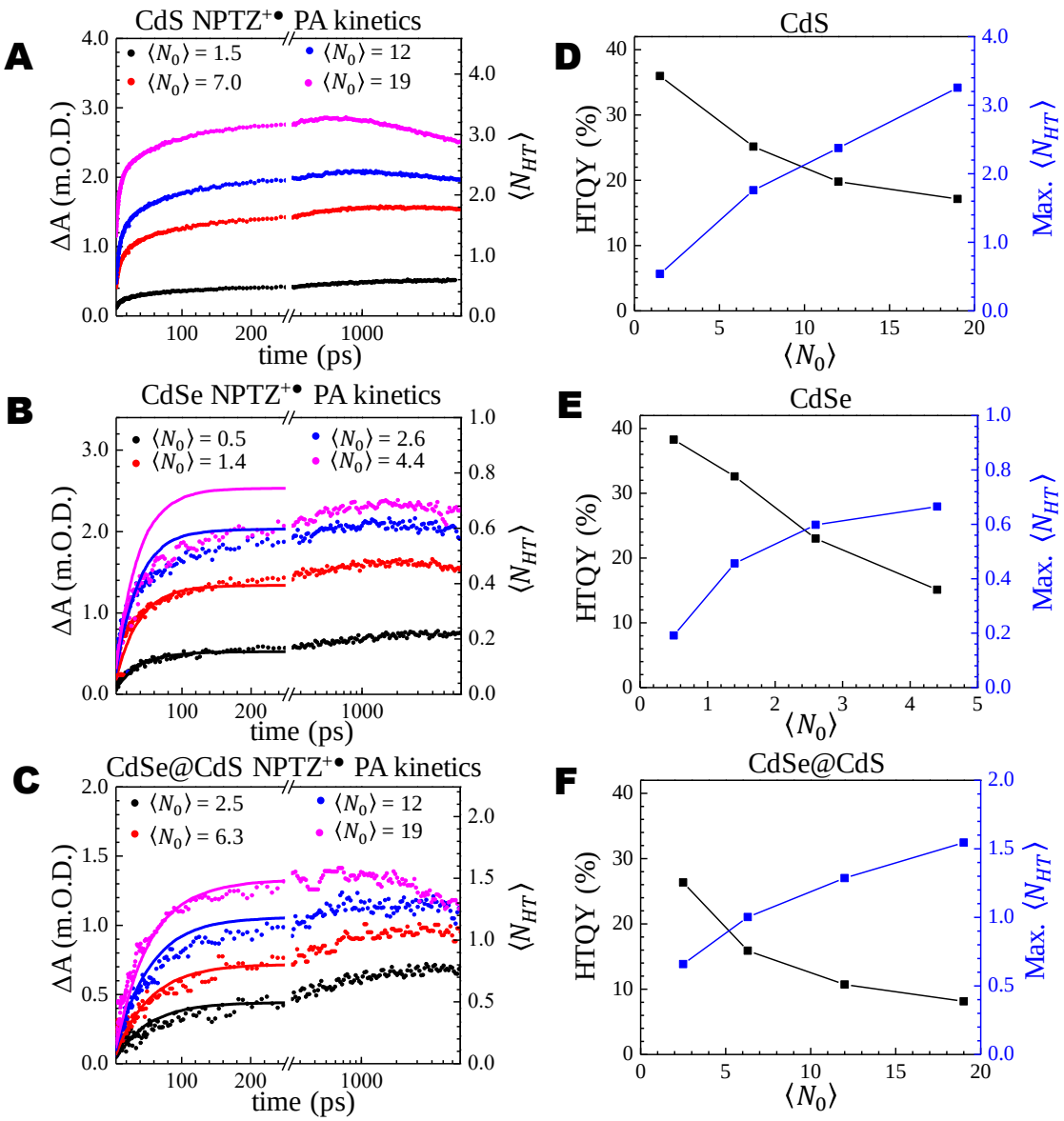

Figure 3. (A-C) TA kinetic traces of $NPTZ^{+\bullet}$ radical population monitored at 650 nm for the three types of QDs excited at various fluences and $\langle N_0 \rangle$. The amplitude of $NPTZ^{+\bullet}$ PA signal was de-convoluted to remove the contribution of the trapped hole PA signal. The left axis is associated with the PA signal amplitude, which is linearly related to the average number of holes transferred per QD, shown by the right axis. Solid lines are the results of the kinetic model with a decoupled trap population. **(D-F)** The hole transfer quantum yield (black) and the maximum number of holes transferred to NPTZ ligands per QD (blue) at each excitation power or $\langle N_0 \rangle$.

For efficient hole transfer to occur at short timescales and under multi-excitonic conditions, the hole transfer rate constant, k_{HT}, should be comparable to the AR rate constant, k_{AR}.[18] The bi-excitonic AR rates determined from native QDs are $(3.0\ ps)^{-1}$, $(22\ ps)^{-1}$, and (35

ps)$^{-1}$ for the CdSe, CdSe/CdS, and CdS QDs, respectively (Table S6). Given the number of excitons per QD as N, k_{AR} scales as $N\cdot(N\text{-}1)$ for the larger CdSe/CdS and CdS QDs; k_{AR} scales as $N^2\cdot(N\text{-}1)$ for the strongly quantum confined 2.5 nm CdSe QDs.[17,18,41] Based on the scaling laws and biexciton AR rates, we can calculate that most of the charge carriers in multi-excitonic QDs will be consumed by AR mechanism within the first 10 ps.

We found here that only the CdS QDs have comparable rates of hole transfer and AR. In Figure 3A, for $\langle N_0 \rangle$ = 7, 12, 19, we can see that the CdS QD is capable of transferring a significant number of holes to NPTZ within the first 10 ps. For $\langle N_0 \rangle$ = 19, ~2 holes can be transferred per CdS QD within 10 ps. In both the CdSe/CdS and the CdSe QDs, k_{AR} well outcompetes k_{HT}, and very few holes are transferred per QD within 10 ps, as seen in Figure 3B and 3C. For the CdSe QDs, the AR lifetime decreases to sub-picosecond level when $\langle N_0 \rangle$ > 2. For the CdSe/CdS QD, k_{AR} is similar to that of the CdS QD, yet k_{HT} is much slower than (10 ps)$^{-1}$ due to the presence of 3ML CdS shell, which forms an energy barrier for the hole to tunnel to the NPTZ ligands. Previously, it had been reported that the hot carriers produced by AR processes could efficiently promote ultrafast electron transfer across energy barriers.[20,21] Here we did not find this mechanism acting efficiently for hole transfer in the CdSe/CdS QDs despite applying conditions with large $\langle N_0 \rangle$ values, presumably because the effective mass of a hole in the VB is much larger than the effective mass of electrons in the CB, and the cooling rate of hot holes is much faster than that of hot electrons.[46] Comparing to the more efficient 5.1 nm CdS QD system, the 2.5 nm CdSe QD has similar hole transfer rates but much faster AR rates; the 3ML CdSe/CdS QD has similar AR rates but much slower hole transfer rates. Therefore, the CdSe and CdSe/CdS QDs investigated here are not able to transfer as many holes per QD as the CdS QDs under multi-excitonic conditions.

The hole transfer quantum yield (HTQY) of the three types of QDs measured at each $\langle N_0 \rangle$ were plotted in Figure 3D-3F. HTQY is defined as the percentage ratio between the maximum number of holes transferred per QD within the 7 ns observation period and the initial number of excitons $\langle N_0 \rangle$. At the lowest value of $\langle N_0 \rangle$ for each type of QD, the HTQY was measured as around 30~40%. We observe the general trend in Figure 3D-3F that the HTQY decreases as $\langle N_0 \rangle$ increases. Due to the very fast k_{AR} of 2.5 nm CdSe, the maximum number of holes transferred per QD has already started to saturate at an $\langle N_0 \rangle$ of 4.4. For the larger CdSe/CdS, the number of holes transferred per QD increases almost proportionally as $\langle N_0 \rangle$ increases but is consistently lower than that of the CdS QD at a similar value of $\langle N_0 \rangle$.

The above analysis based on the scaling law of k_{AR} indicates that the hole transfer rates during the period of 10-100 ps would be largely independent of excitation fluences for multi-excitonic QDs with large $\langle N_0 \rangle$ values. However, data for all the QDs in Figure 3A-3C show that both the hole transfer rate and the number of holes transferred during the period of 10-100 ps increases as $\langle N_0 \rangle$ increases. Roughly 0.5-1.5 holes were transferred to NPTZ per QD transferred in the 10-100 ps period, depending on $\langle N_0 \rangle$. For CdSe and CdSe/CdS QDs, nearly all of hole transfer takes place in this period. For CdS QDs, because the hole transfer rate is competitive with the AR rate, both the holes transferred in the first 10 ps and the holes transferred in the 10-100 ps contribute significantly to the overall number of transferred holes. The observed fluence dependence indicates that multiple carriers must remain on these QDs for longer timescales than expected.

With the introduction of NPTZ ligands, we postulate that multi-exciton dissociation during AR events cause holes to populate surface trap states that are de-coupled from the native states of the QD (Figure 4A). These hole trapping states are likely formed as a result of the presence of hole accepting ligands and, thus, have much weaker electron-hole coupling as compared to the electron-hole pair forming an exciton or charges in shallow traps. The de-coupling of the new hole trapping states from native QD states, similar to a charge-separated state, can result in long carrier lifetimes since AR is suppressed. In this mechanism, though the hole transfer rate is generally slower than AR kinetics, holes can first accumulate in the de-coupled surface traps and then further transfer to NPTZ over longer time periods.

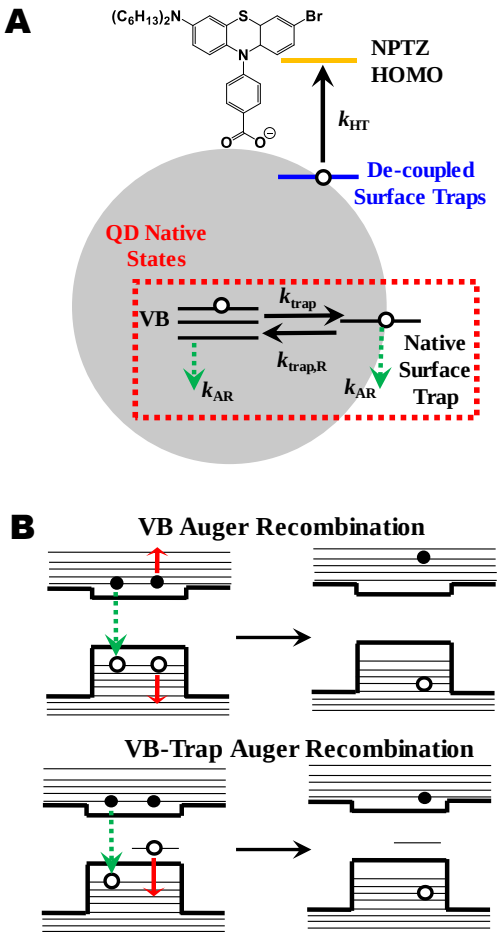

Figure 4. A) A schematic showing the energy levels involved in modeling the kinetics of hole transfer and hole trapping under multi-excitonic conditions. **B)** Auger channels considered for QDs with hole trapping states. The three red arrows are associated with three different trion channels.

To corroborate this mechanism, we simulated the kinetics of trap-mediated hole transfer. The hole transfer rate constants from de-coupled surface trap states to the NPTZ ligand were extracted from the data of the first 100 ps of the lowest $\langle N_0 \rangle$ for each of the three types of QDs (black kinetic traces in Figure 3A-3C) with a single exponential functional form. The obtained rate constants are $(31\pm3\ \text{ps})^{-1}$, $(73\pm20\ \text{ps})^{-1}$, and $(27\pm2\ \text{ps})^{-1}$ for CdSe, CdSe/CdS, and CdS QDs, respectively. Simulating transfer from a population of de-coupled trap states to the NPTZ ligands using the extracted rates and an initial trapped hole population determined to simultaneously fit the NPTZ and hole trap PA signals (see below) shows good agreement with the hole transfer dynamics on CdSe and CdSe/CdS QDs as short time transfer is not significant for these particles. The modeling of the CdS QDs is more difficult, because the significant contribution of short time transfer means that the trap-mediated mechanism cannot account for the full dynamics of hole transfer in this system and other pathways such as direct transfer from VB can also be important.

The long-lived charge carriers are important for improving the efficiency of multi-excitonic hole transfer. The overall results here demonstrate that, in general, QDs with longer AR lifetimes and faster hole transfer rates are preferred for promoting rapid hole transfer under multi-excitonic conditions. However, the observed fluence-dependence of intermediate timescale transfer suggests that the AR kinetics can be circumvented by the long-lived trapping of multiple holes. This effect motivated further analysis of the kinetics of trapped holes under multi-excitonic conditions.

The Role of Hole Traps in Promoting Hole Transfer from Multi-Excitonic QDs

Figure 5 illustrates the PA signal at 710 nm of trapped holes in both native (panels A and B) and NPTZ functionalized quantum dots (panels C and D). The population of trapped holes in the native CdSe and CdSe/CdS QDs decays rapidly before converging to a long-lived plateau level, which represents the single-excitonic state. Most of the trapped holes are consumed within the first 10 ps on a timescale consistent with AR scaling laws and matching the CB bleaching kinetics (Figure S16). This observation indicates that these traps participate in AR. In contrast, for the QDs with the NPTZ hole acceptors, the population decay slows to timescales of 10s~100s ps, and the population plateaus at a level dependent on $\langle N_0 \rangle$. Compared to the kinetics in Figure 5A and 5B, the PA signals of QDs with NPTZ ligands also showed maxima at later times with different amplitudes. These comparisons indicate that the nature of the trapped holes is different from those in the native QDs. The decay curves measured at 710 nm for CdS QDs show similar contrasts between native QDs and QDs with NPTZ ligands (Figures S18-S19).

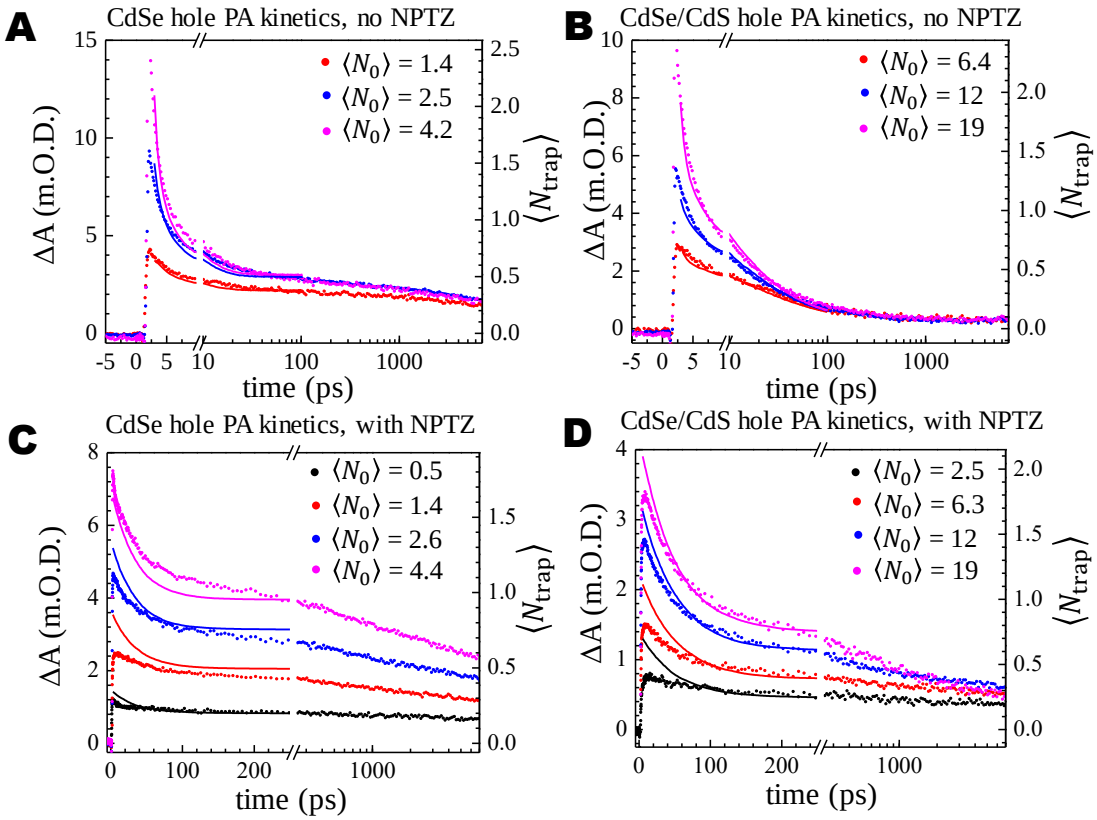

Figure 5. TA kinetic traces of the PA signals at 710 nm measured at a series of $\langle N_0 \rangle$ displayed for CdSe QDs with native oleate ligands **(A)**, and with NPTZ ligands **(C)**; CdSe/CdS QDs with native oleate ligands **(B)**, and with NPTZ ligands **(D)**. The modeled kinetics of trapped holes shown as solid lines through the data points of TA signal at 710 nm. The left axis refers to the measured PA signal amplitude, and the right axis refers to the estimated number of trapped holes associated with the optical signal.

For the CdSe and CdSe/CdS QDs, we apply our kinetic models to understand the observed hole transfer kinetics in terms of trapping (k_{trap}), de-trapping ($k_{\mathrm{trap,R}}$), AR (k_{AR}), and hole transfer (k_{HT}) rates. As shown in Figure 4A, these are the important processes that control the dynamics of holes in these QD systems. To understand mechanisms by which these hole populations can decay, we examined possible AR channels in a QD containing hole trapping states. As shown by the red arrows in the upper panel of Figure 4B, AR between two excitons can be decomposed to the hole channel, where the recombination of an exciton produces a hot hole, and the electron channel, where recombination produces a hot electron.[41] In our model for native QDs, a trapped hole can participate in AR via a modified hole channel, where the recombination of a VB hole and an electron promotes the trapped hole deep into the VB, as shown as the VB-trap AR channel in Figure 4B. We found through semi-empirical pseudopotential calculations that the VB-trap channel has a comparable rate to the VB channels (Table S7).[47,48] Calculations also show that, in general, other channels involving the recombination of a trapped hole and an electron are orders of magnitude slower. In the simplest model, the three channels in Figure 4B have the same rate constant, which can be extracted from analyzing the XB bleaching signal under band-edge excitation conditions. After specifying these AR channels and their scaling relationships relative to hole populations in the trap and VB, a set of coupled differential equations describing the hole populations were solved by running trajectories with a Monte Carlo approach. Tables of all the modeling parameters in this section are given in the SI (Tables S7-S10).

The initial conditions of the kinetic model were chosen such that the total number of holes is close to $\langle N_0 \rangle$ determined from experiments. For the native QDs, the shape of the simulated decay curve is largely governed by the trapping and de-trapping rates, as these rates control the distribution of total hole population into the VB and traps which determine the overall AR rates of the system. Literature results and the observed rapid rise of the trap signal informs that the hole trapping rate in the model should be set as faster than $(1\ \text{ps})^{-1}$.[38,49] To globally fit the experimental data across a range of $\langle N_0 \rangle$ and prevent excessive trapping to slow the simulated decay curves, the de-trapping rate has to be comparable to the trapping rate, allowing the trapped holes to establish a rapid equilibrium with the VB holes. In Figure 5A and 5B, the modeling results of the first 100 ps using parameters fit within these constraints agree well with experimental data. For CdSe QDs, the kinetic model estimates that the number of holes in the VB is comparable to the number of trapped holes, $\langle N_{\text{trap}} \rangle$, represented by the TA signal amplitude at 710 nm. For CdSe/CdS QDs, the majority of holes remain on the VB while only a few holes were trapped, which is consistent with the disfavored energetics of trapping states on CdS surface versus the energy of the CdSe VB.[32] It is important to note here that the equilibrium model employed here focuses on the ultrafast multi-carrier dynamics on the picosecond timescale, and much slower non-radiative and radiative events on the nanosecond timescale are not included in the model. For a single-excitonic QD, the trapping could become irreversible at longer timescales and cause the photoluminescence quantum yield to decrease.

In Figure 5C and 5D, the fast equilibration between VB and trapped holes is not consistent with the trapped hole PA signals observed in QDs functionalized with NPTZ ligands. When the hole acceptors are present, the decay rates of trapped hole population decrease significantly. The kinetic model for QDs with NPTZ ligands needs to account for kinetic data of

both the $NPTZ^{+\bullet}$ at 650 nm and trapped holes at 710 nm. The model where the population of $NPTZ^{+\bullet}$ was coupled to the trapped hole population of the native QD model described above could not match the experimental data (Figure S29), even when trapping, de-trapping, or hole transfer rates were adjusted. The failure of the coupled model indicates that the trapped holes in QDs with NPTZ ligands are kinetically de-coupled from VB. It is possible that hole accepting ligands such as NPTZ alter the energy levels of trapping sites of native QDs or create new trapping sites as they replace the oleate ligands on QD surface. Previous work on hole accepting ligands has shown that their attachment to QDs can produce surface states that are localized toward these ligands.[33] These new trapping states could also be unable to participate in the VB-trap AR channel because their wave function becomes much more separated from carriers in CB and VB states than traps in native QDs, therefore effectively acting as a charge-separated state.

Modeling results indicate that holes in the de-coupled traps provide the long-lived carrier reservoir responsible for the fluence-dependent hole transfer to NPTZ ligands after 10 ps observed in Figure 3. Within the limit of no trapping and de-trapping equilibration, the kinetic model reduces to a set of two coupled equations describing the population of trapped holes and the population of $NPTZ^{+\bullet}$, which are connected by simple exponential hole transfer from the trapping sites to the NPTZ ligands. Following energetic events at early times such as Auger-assisted trapping[50] or direct cooling of carriers, the de-coupled trapping sites become populated with a number of holes. These trapped holes would not be annihilated by AR events and would account for the gradual transfer to NPTZ ligands after 10 ps as observed in Figure 3.

In Figure 5C and 5D, the PA signal shows fluence-dependent plateau levels that last hundreds of ps. The plateau phenomena suggest that only a fraction of the trapped holes can be transferred to NPTZ acceptors. Therefore, the trapped hole population is further divided into

'active' holes which can transfer to NPTZ, and 'passive' holes which are unable to transfer during our observation time window due to kinetic barriers, such as the hole being localized at a trap state far from a NPTZ ligand. Since the surface coverage of NPTZ is only ~20%, the holes trapped at sites which are not adjacent to a NPTZ ligand would need to undergo a series of slow hole hopping events to reach NPTZ ligands, which have been measured to occur over timescales longer than several nanoseconds.[38,51,52] The initial number of trapped holes, $\langle N_{\mathrm{trap}} \rangle$, and the fraction of active traps are fitting parameters for the model. The fraction of active traps falls around 50%, and is held constant across excitation fluences to allow for the model to capture the plateau levels.

The fitting lines in Figure 3 and Figure 5, using fitting parameters consistent with both $NPTZ^{+\bullet}$ and trapped hole PA data, show that the decay of the trapped hole population within the first 250 ps can be largely accounted for by the rise of the $NPTZ^{+\bullet}$ population across various excitation fluences. In the modeling of these NPTZ modified systems, the valence band and the traps are assumed to be completely decoupled. There may, however, still be some level of de-trapping or AR occurring at reduced rates compared to the native QDs, which may account for some of the discrepancies between model and experimental kinetics. For instance, in the case of CdSe with $\langle N_0 \rangle$ = 4.4, the simulated decay of trapped holes in Figure 5C clearly causes the simulated growth of $NPTZ^{+\bullet}$ population in Figure 3B to largely miss the experimental trace, suggesting that some trapped holes could be annihilated by AR without transferring to the NPTZ. Nevertheless, the de-coupled nature of the simplified model captures the major features of the observed decay kinetics and shows large contrast to the coupled model that describes native QDs. This kinetic model allowed us to identify long-lived trapped holes as the reservoir of carrier responsible for the observed fluence dependent hole transfer at intermediate times.

Trapping a large number of holes at early times can then be a key to achieving high HTQYs under multi-excitonic conditions, as the holes in these de-coupled trapping states have long lifetimes. In the CdSe and CdSe/CdS QDs studied here, the model suggests that the number of holes trapped is yet only a small fraction of $\langle N_0 \rangle$, resulting in the limited HTQY.

Conclusions

In summary, we have applied ultrafast TA spectroscopy to examine the hole transfer dynamics from three types of cadmium chalcogenide QDs to NPTZ ligands under multi-excitonic conditions. The results indicate that the transfer of multiple holes from QDs to molecular acceptors at short times is possible when the hole transfer rate and AR rate are comparable. Furthermore, the hole transfer mediated by trapping states occurs on the timescale of 10s-100s ps, much longer than the AR lifetimes of the QDs studied here. Modeling of the kinetics data suggest a two-stage transfer mechanism. First, holes can directly transfer to NPTZ ligands under the short lived multi-excitonic state. Next, multiple irreversibly trapped holes in the de-coupled trapping states with long AR lifetimes can gradually transfer charge to acceptors. The results here suggest that careful engineering of hole trap states both in number and kind is required in order to achieve effective hole transfer over non-radiative recombination events when QDs are operating in the multi-excitonic regime.

Methods/Experimental

Synthesis. QDs were synthesized based on previously published protocols with full description in the SI. For the CdS QDs, 4.0 nm QDs were first synthesized,[31] then 5.1 nm QDs were obtained by a second injection to enlarge the 4.0 nm QDs. For the CdSe QDs, we first

synthesized 2.3 nm QDs with phosphonic acid ligand shells, then performed z-type ligand exchange to obtain the 2.5 nm oleate-capped QDs.[53,54] The 3ML CdSe/CdS QDs were prepared by the slow growth of CdS shells onto 2.3 nm CdSe cores.[55] All the QDs were capped with oleate ligands to allow the binding of NPTZ ligands. The details of the four-step synthesis of NPTZ from phenothiazine were given in SI. The structure of NPTZ was confirmed by mass spectrum and NMR analysis (^{1}H and ^{13}C).

^{1}H NMR Measurements. The ligand compositions of the native QDs and QDs bound with NPTZ ligands were quantified by a Bruker 700 MHz spectrometer using 1% mesitylene as internal standard in d_8-toluene. The surface coverage of NPTZ was determined by two methods[31] which gave virtually the same results. Method (i) counted the number of oleate ligands displaced by NPTZ from QD surface; method (ii) counted the number of NPTZ molecules bound to the QD surface. The results were listed in SI, and demonstrated 1-to-1 ligand exchange between oleaic acid and NPTZ.

TA Measurements. The ultrafast TA experiments were performed with a tunable-wavelength pump and white-light probe with varying pump-probe delay times, as described in a previous work.[55] The pump beam was generated by a Coherent OperA optical parametric amplifier pumped by a 1 kHz pulse train (~50 fs duration, centered at 800 nm) from a regeneratively amplified Ti: sapphire oscillator (Coherent Libra). The pump beam tuned at a certain wavelength, e.g. 415 nm, was chopped by a mechanical chopper at 500 Hz. For TA spectra recorded in the wavelength range 350-550 nm, the white-light continuum probe was generated by focusing a fraction of the 800 nm beam onto a translating CaF_2 substrate. For TA spectra recorded in the wavelength range 500-750 nm, the white-light continuum probe was generated by focusing the 800 nm probe beam into a sapphire substrate. The time-resolved differential

extinction spectra were collected with a commercial Helios absorption spectrometer (Ultrafast Systems LLC). The delay between the probe and pump pulses was controlled by a linear translation stage. All the QD samples for TA measurements were prepared in a N_2 glovebox by diluting the native QD or QD-NPTZ stock solution with d_8-toluene until the optical density at 415 nm reached ~0.2. The diluted solution was sealed in a 2 mm quartz cuvette equipped with a gas-tight screw cap before transferred out for TA measurements. UV-visible spectra were acquired before and after TA measurements to show no spectral changes or photo-degradation of QDs and NPTZ molecules had occurred.

Kinetic Modeling of AR and Hole Transfer Dynamics. The dynamics of AR and hole transfer were simulated by solving a kinetic master equation that incorporates all the important processes for describing hole dynamics on a given QD including AR, trapping, de-trapping, and hole transfer in the case of NPTZ modified QDs. This equation was solved via the Gillespie algorithm,[56] a trajectory based Monte Carlo method for solving coupled differential equations, with rates and initial conditions fit to the experimental data. A detailed discussion of the development of the model, along with tables of parameters, can be found in the Supporting Information.

Calculation of AR Lifetimes. As in previous work[57] CdSe QD structures were obtained by cleaving bulk wurtzite CdSe crystals and then optimizing the resulting structure via the LAMMPS molecular dynamics code[58] using Stillinger-Weber interatomic potentials.[59] The outer layer was then removed and the subsequent monolayer was replaced by ligand potentials to represent the passivation layer. Surface hole traps were modeled by the removal of a passivation ligand from a Se atom on the surface, which creates a localized trap state. Electronic structure calculations were performed using the semiempirical pseudopotential method.[48] The filter diagonalization technique was used to find quasiparticle states near the band edge, which were used as input to the

Bethe−Salpeter equation to obtain correlated excitonic states. The biexcitonic AR lifetime was computed using Fermi's golden rule, with an average over thermally distributed initial biexcitonic states.

Associated Content

The Supporting Information is available free of charge at https://pubs.acs.org/.
Details of synthesis and materials characterization, additional TA data and analysis, and theoretical modeling method (PDF)

Acknowledgement

This work was supported by the U.S. Department of Energy, Office of Science, Office of Basic Energy Sciences, Materials Sciences and Engineering Division, under Contract No. DE-AC02-05-CH11231 within the Physical Chemistry of Inorganic Nanostructures Program (KC3103). Work at the Molecular Foundry was supported by the Office of Science, Office of Basic Energy Sciences, of the U.S. Department of Energy under Contract No. DE-AC02-05-CH11231. We also acknowledge the National Energy Research Scientific Computing Center (NERSC), a U.S. Department of Energy Office of Science User Facility operated under Contract No. DE–AC02–05CH11231. D.J. acknowledges the support of the Computational Science Graduate Fellowship from the U.S. Department of Energy under Grant No. DE- SC0019323. We thank Dr. Anna Wuttig for assisting the cyclic voltammetry measurements.

References

(1) Caruge, J. M.; Halpert, J. E.; Wood, V.; Buloví, V.; Bawendi, M. G. Colloidal Quantum-Dot Light-Emitting Diodes with Metal-Oxide Charge Transport Layers. *Nat. Photonics* **2008**, *2* (4), 247–250.

(2) Roh, J.; Park, Y. S.; Lim, J.; Klimov, V. I. Optically Pumped Colloidal-Quantum-Dot Lasing in LED-like Devices with an Integrated Optical Cavity. *Nat. Commun.* **2020**, *11* (1), 1–10.

(3) Jr. Bruchez, M.; Moronne, M.; Gin, P.; Weiss, S.; Alivisatos, A. P. Semiconductor Nanocrystals as Fluorescent Biological Labels. *Science* **1998**, *281* (5385), 2013–2016.

(4) Kairdolf, B. A.; Smith, A. M.; Stokes, T. H.; Wang, M. D.; Young, A. N.; Nie, S. Semiconductor Quantum Dots for Bioimaging and Biodiagnostic Applications. *Annu. Rev. Anal. Chem.* **2013**, *6* (1), 143–162.

(5) Baek, S. W.; Jun, S.; Kim, B.; Proppe, A. H.; Ouellette, O.; Voznyy, O.; Kim, C.; Kim, J.; Walters, G.; Song, J. H.; Jeong, S.; Byun, H. R.; Jeong, M. S.; Hoogland, S.; García de Arquer, F. P.; Kelley, S. O.; Lee, J. Y.; Sargent, E. H. Efficient Hybrid Colloidal Quantum Dot/Organic Solar Cells Mediated by near-Infrared Sensitizing Small Molecules. *Nat. Energy* **2019**, *4* (11), 969–976.

(6) Bronstein, N. D.; Yao, Y.; Xu, L.; O'Brien, E.; Powers, A. S.; Ferry, V. E.; Alivisatos, A. P.; Nuzzo, R. G. Quantum Dot Luminescent Concentrator Cavity Exhibiting 30-Fold Concentration. *ACS Photonics* **2015**, *2* (11), 1576–1583.

(7) Wolff, C. M.; Frischmann, P. D.; Schulze, M.; Bohn, B. J.; Wein, R.; Livadas, P.; Carlson, M. T.; Jäckel, F.; Feldmann, J.; Würthner, F.; Stolarczyk, J. K. All-in-One Visible-Light-Driven Water Splitting by Combining Nanoparticulate and Molecular Co-Catalysts on CdS Nanorods. *Nat. Energy* **2018**, *3* (10), 862–869.

(8) Wu, K.; Lian, T. Quantum Confined Colloidal Nanorod Heterostructures for Solar-to-Fuel Conversion. *Chem. Soc. Rev.* **2016**, *45* (14), 3781–3810.

(9) Harris, R. D.; Bettis Homan, S.; Kodaimati, M.; He, C.; Nepomnyashchii, A. B.; Swenson, N. K.; Lian, S.; Calzada, R.; Weiss, E. A. Electronic Processes within Quantum Dot-Molecule Complexes. *Chem. Rev.* **2016**, *116* (21), 12865–12919.

(10) Ben-Shahar, Y.; Scotognella, F.; Kriegel, I.; Moretti, L.; Cerullo, G.; Rabani, E.; Banin, U. Optimal Metal Domain Size for Photocatalysis with Hybrid Semiconductor-Metal Nanorods. *Nat. Commun.* **2016**, *7*, 1–7.

(11) Amirav, L.; Alivisatos, A. P. Photocatalytic Hydrogen Production with Tunable Nanorod Heterostructures. *J. Phys. Chem. Lett.* **2010**, *1* (7), 1051–1054.

(12) Lian, S.; Kodaimati, M. S.; Weiss, E. A. Photocatalytically Active Superstructures of Quantum Dots and Iron Porphyrins for Reduction of CO_2 to CO in Water. *ACS Nano* **2018**, *12*, 568–575.

(13) Kuehnel, M. F.; Orchard, K. L.; Dalle, K. E.; Reisner, E. Selective Photocatalytic CO_2 Reduction in Water through Anchoring of a Molecular Ni Catalyst on CdS Nanocrystals. *J. Am. Chem. Soc.* **2017**, *139*, 7217–7223.

(14) Jiang, Y.; Wang, C.; Rogers, C. R.; Kodaimati, M. S.; Weiss, E. A. Regio- and Diastereoselective Intermolecular [2+2] Cycloadditions Photocatalysed by Quantum Dots. *Nat. Chem.* **2019**, *11*, 1034–1040.

(15) Caputo, J. A.; Frenette, L. C.; Zhao, N.; Sowers, K. L.; Krauss, T. D.; Weix, D. J. General and Efficient C-C Bond Forming Photoredox Catalysis with Semiconductor Quantum Dots. *J. Am. Chem. Soc.* **2017**, *139* (12), 4250–4253.

(16) Verbitsky, L.; Waiskopf, N.; Magdassi, S.; Banin, U. A Clear Solution: Semiconductor

Nanocrystals as Photoinitiators in Solvent Free Polymerization. *Nanoscale* **2019**, *11* (23).

(17) Klimov, V. I. Spectral and Dynamical Properties of Multiexcitons in Semiconductor Nanocrystals. *Annu. Rev. Phys. Chem.* **2007**, *58*, 635–673.

(18) Zhu, H.; Yang, Y.; Lian, T. Multiexciton Annihilation and Dissociation in Quantum Confined Semiconductor Nanocrystals. *Acc. Chem. Res.* **2013**, *46* (6), 1270–1279..

(19) Zhu, H.; Song, N.; Rodríguez-Córdoba, W.; Lian, T. Wave Function Engineering for Efficient Extraction of up to Nineteen Electrons from One CdSe/CdS Quasi-Type II Quantum Dot. *J. Am. Chem. Soc.* **2012**, *134* (9), 4250–4257.

(20) Ben-Shahar, Y.; Philbin, J. P.; Scotognella, F.; Ganzer, L.; Cerullo, G.; Rabani, E.; Banin, U. Charge Carrier Dynamics in Photocatalytic Hybrid Semiconductor-Metal Nanorods: Crossover from Auger Recombination to Charge Transfer. *Nano Lett.* **2018**, *18* (8), 5211–5216.

(21) Gao, J.; Kidon, L.; Rabani, E.; Alivisatos, A. P. Ultrahigh Hot Carrier Transient Photocurrent in Nanocrystal Arrays by Auger Recombination. *Nano Lett.* **2019**, *19* (7), 4804–4810..

(22) Young, R. M.; Jensen, S. C.; Edme, K.; Wu, Y.; Krzyaniak, M. D.; Vermeulen, N. A.; Dale, E. J.; Stoddart, J. F.; Weiss, E. A.; Wasielewski, M. R.; Co, D. T. Ultrafast Two-Electron Transfer in a CdS Quantum Dot-Extended-Viologen Cyclophane Complex. *J. Am. Chem. Soc.* **2016**, *138* (19), 6163–6170.

(23) Matylitsky, V. V.; Dworak, L.; Breus, V. V.; Basche, T.; Wachtveitl, J. Ultrafast Charge Separation in Multiexcited CdSe Quantum Dots Mediated by Adsorbed Electron Acceptors. *J. Am. Chem. Soc.* **2009**, *131* (7), 2424–2425.

(24) Huang, J.; Huang, Z.; Yang, Y.; Zhu, H.; Lian, T. Multiple Exciton Dissociation in CdSe

Quantum Dots by Ultrafast Electron Transfer to Adsorbed Methylene Blue. *J. Am. Chem. Soc.* **2010**, *132* (13), 4858–4864.

(25) Yang, Y.; Rodríguez-Córdoba, W.; Lian, T. Multiple Exciton Generation and Dissociation in PbS Quantum Dot-Electron Acceptor Complexes. *Nano Lett.* **2012**, *12* (8), 4235–4241.

(26) Luo, X.; Liang, G.; Wang, J.; Liu, X.; Wu, K. Picosecond Multi-Hole Transfer and Microsecond Charge-Separated States at the Perovskite Nanocrystal/Tetracene Interface. *Chem. Sci.* **2019**, *10* (8), 2459–2464.

(27) Olshansky, J. H.; Ding, T. X.; Lee, Y. V; Leone, S. R.; Alivisatos, A. P. Hole Transfer from Photoexcited Quantum Dots: The Relationship between Driving Force and Rate. *J. Am. Chem. Soc.* **2015**, *137* (49), 15567–15575.

(28) Aldana, J.; Wang, Y. A.; Peng, X. Photochemical Instability of CdSe Nanocrystals Coated by Hydrophilic Thiols. *J. Am. Chem. Soc.* **2001**, *123* (36), 8844–8850.

(29) Califano, M.; Franceschetti, A.; Zunger, A. Temperature Dependence of Excitonic Radiative Decay in CdSe Quantum Dots: The Role of Surface Hole Traps. *Nano Lett.* **2005**, *5* (12), 2360–2364.

(30) Giansante, C.; Infante, I. Surface Traps in Colloidal Quantum Dots: A Combined Experimental and Theoretical Perspective. *J. Phys. Chem. Lett.* **2017**, *8* (20), 5209–5215.

(31) Lian, S.; Weinberg, D. J.; Harris, R. D.; Kodaimati, M. S.; Weiss, E. A. Subpicosecond Photoinduced Hole Transfer from a CdS Quantum Dot to a Molecular Acceptor Bound Through an Exciton-Delocalizing Ligand. *ACS Nano* **2016**, *10* (6), 6372–6382.

(32) Olshansky, J. H.; Balan, A. D.; Ding, T. X.; Fu, X.; Lee, Y. V; Alivisatos, A. P. Temperature-Dependent Hole Transfer from Photoexcited Quantum Dots to Molecular Species: Evidence for Trap-Mediated Transfer. *ACS Nano* **2017**, *11* (8), 8346–8355.

(33) Tarafder, K.; Surendranath, Y.; Olshansky, J. H.; Alivisatos, A. P.; Wang, L.-W. Hole Transfer Dynamics from a CdSe/CdS Quantum Rod to a Tethered Ferrocene Derivative. *J. Am. Chem. Soc.* **2014**, *136* (13), 5121–5131.

(34) Tyagi, P.; Kambhampati, P. False Multiple Exciton Recombination and Multiple Exciton Generation Signals in Semiconductor Quantum Dots Arise from Surface Charge Trapping. *J. Chem. Phys.* **2011**, *134* (9), 094706.

(35) Walsh, B. R.; Saari, J. I.; Krause, M. M.; Nick, R.; Coe-Sullivan, S.; Kambhampati, P. Surface and Interface Effects on Non-Radiative Exciton Recombination and Relaxation Dynamics in CdSe/Cd,Zn,S Nanocrystals. *Chem. Phys.* **2016**, *471*, 11–17.

(36) He, Y.; Hu, S.; Han, T.; Chen, X.; Yu, Y.; Li, T.; Zhu, W.; Ouyang, G. Suppression of the Auger Recombination Process in CdSe/CdS Core/Shell Nanocrystals. *ACS Omega* **2019**, *4* (5), 9198–9203.

(37) Lian, S.; Christensen, J. A.; Kodaimati, M. S.; Rogers, C. R.; Wasielewski, M. R.; Weiss, E. A. Oxidation of a Molecule by the Biexcitonic State of a CdS Quantum Dot. *J. Phys. Chem. C* **2019**, *123* (10), 5923–5930.

(38) Wu, K.; Du, Y.; Tang, H.; Chen, Z.; Lian, T. Efficient Extraction of Trapped Holes from Colloidal CdS Nanorods. *J. Am. Chem. Soc.* **2015**, *137* (32), 10224–10230.

(39) Frantsuzov, P.; Kuno, M.; Jankó, B.; Marcus, R. A. Universal Emission Intermittency in Quantum Dots, Nanorods and Nanowires. *Nat. Phys.* **2008**, *4* (7), 519–522.

(40) Efros, A. L.; Rosen, M. Random Telegraph Signal in the Photoluminescence Intensity of a Single Quantum Dot. *Phys. Rev. Lett.* **1997**, *78* (6), 1110–1113.

(41) Philbin, J. P.; Rabani, E. Auger Recombination Lifetime Scaling for Type I and Quasi-Type II Core/Shell Quantum Dots. *J. Phys. Chem. Lett.* **2020**, *11* (13), 5132–5138.

(42) Eshet, H.; Grünwald, M.; Rabani, E. The Electronic Structure of CdSe/CdS Core/Shell Seeded Nanorods: Type-I or Quasi-Type-II? *Nano Lett.* **2013**, *13* (12), 5880–5885.

(43) Sitt, A.; Sala, F. Della; Menagen, G.; Banin, U. Multiexciton Engineering in Seeded Core/Shell Nanorods: Transfer from Type-I to Quasi-Type-II Regimes. *Nano Lett.* **2009**, *9* (10), 3470–3476.

(44) Jasrasaria, D.; Philbin, J. P.; Yan, C.; Weinberg, D.; Alivisatos, A. P.; Rabani, E. Sub-Bandgap Photoinduced Transient Absorption Features in CdSe Nanostructures: The Role of Trapped Holes. *J. Phys. Chem. C* **2020**, *124* (31), 17372–17378.

(45) Schnitzenbaumer, K. J.; Labrador, T.; Dukovic, G. Impact of Chalcogenide Ligands on Excited State Dynamics in CdSe Quantum Dots. *J. Phys. Chem. C* **2015**, *119* (23), 13314–13324.

(46) Laheld, U. E. H.; Einevoll, G. T. Excitons in CdSe Quantum Dots. *Phys. Rev. B* **1997**, *55* (8), 5184–5204.

(47) Wang, L.-W.; Zunger, A. Pseudopotential Calculations of Nanoscale CdSe Quantum Dots. *Phys. Rev. B* **1996**, *53* (15), 9579–9582.

(48) Rabani, E.; Hetényi, B.; Berne, B. J.; Brus, L. E. Electronic Properties of CdSe Nanocrystals in the Absence and Presence of a Dielectric Medium. *J. Chem. Phys.* **1999**, *110* (11), 5355–5369.

(49) McArthur, E. A.; Morris-Cohen, A. J.; Knowles, K. E.; Weiss, E. A. Charge Carrier Resolved Relaxation of the First Excitonic State in CdSe Quantum Dots Probed with Near-Infrared Transient Absorption Spectroscopy. *J. Phys. Chem. B* **2010**, *114* (45), 14514–14520.

(50) Klimov, V. I.; McBranch, D. W. Auger-Process-Induced Charge Separation in

Semiconductor Nanocrystals. *Phys. Rev. B* **1997**, *55* (19), 13173–13179.

(51) Utterback, J. K.; Hamby, H.; Pearce, O. M.; Eaves, J. D.; Dukovic, G. Trapped-Hole Diffusion in Photoexcited CdSe Nanorods. *J. Phys. Chem. C* **2018**, *122* (29), 16974–16982.

(52) Utterback, J. K.; Grennell, A. N.; Wilker, M. B.; Pearce, O. M.; Eaves, J. D.; Dukovic, G. Observation of Trapped-Hole Diffusion on the Surfaces of CdS Nanorods. *Nat. Chem.* **2016**, *8* (11), 1061–1066.

(53) Balan, A. D.; Olshansky, J. H.; Horowitz, Y.; Han, H.-L.; O'Brien, E. A.; Tang, L.; Somorjai, G. A.; Alivisatos, A. P. Unsaturated Ligands Seed an Order to Disorder Transition in Mixed Ligand Shells of CdSe/CdS Quantum Dots. *ACS Nano* **2019**, *13* (12), 13784–13796.

(54) Carbone, L.; Nobile, C.; De Giorgi, M.; Sala, F. Della; Morello, G.; Pompa, P.; Hytch, M.; Snoeck, E.; Fiore, A.; Franchini, I. R.; Nadasan, M.; Silvestre, A. F.; Chiodo, L.; Kudera, S.; Cingolani, R.; Krahne, R.; Manna, L. Synthesis and Micrometer-Scale Assembly of Colloidal CdSe/CdS Nanorods Prepared by a Seeded Growth Approach. *Nano Lett.* **2007**, *7* (10), 2942–2950.

(55) Hanifi, D. A.; Bronstein, N. D.; Koscher, B. A.; Nett, Z.; Swabeck, J. K.; Takano, K.; Schwartzberg, A. M.; Maserati, L.; Vandewal, K.; van de Burgt, Y.; Salleo, A.; Alivisatos, A. P. Redefining Near-Unity Luminescence in Quantum Dots with Photothermal Threshold Quantum Yield. *Science* **2019**, *363* (6432), 1199 – 1202.

(56) Gillespie, D. T. Exact Stochastic Simulation of Coupled Chemical Reactions. *J. Phys. Chem.* **1977**, *81* (25), 2340–2361.

(57) Ondry, J. C.; Philbin, J. P.; Lostica, M.; Rabani, E.; Alivisatos, A. P. Resilient Pathways to

Atomic Attachment of Quantum Dot Dimers and Artificial Solids from Faceted CdSe Quantum Dot Building Blocks. *ACS Nano* **2019**, *13* (11), 12322–12344.

(58) Plimpton, S. Fast Parallel Algorithms for Short-Range Molecular Dynamics. *J. Comput. Phys.* **1995**, *117* (1), 1–19.

(59) Zhou, X. W.; Ward, D. K.; Martin, J. E.; van Swol, F. B.; Cruz-Campa, J. L.; Zubia, D. Stillinger-Weber Potential for the II-VI Elements Zn-Cd-Hg-S-Se-Te. *Phys. Rev. B* **2013**, *88* (8), 85309.

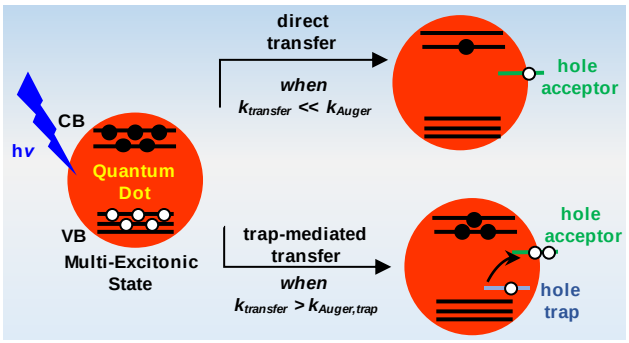

For Table of Contents Only